Assisting Gait Stability in Walking Aid Users Exploiting Biomechanical Variables Correlation

Andrea Fortuna, *Graduate Student Member, IEEE*, Marta Lorenzini, *Member, IEEE*, Younggeol Cho, *Member, IEEE*, Robin Arbaud, Stefano Filippo Castiglia, Mariano Serrao, Alberto Ranavalo, Elena De Momi, *Senior Member, IEEE*, and Arash Ajoudani, *Member, IEEE*

***Abstract*—Walking aids for individuals with musculoskeletal frailty or motor disabilities must ensure adequate physical support and assistance to their users. To this end, sensor-enabled human state monitoring and estimation are crucial. This letter proposes an innovative approach to assessing users' stability while walking with WANDER, a novel gait assistive device, by exploiting the correlation between the eXtrapolated Center of Mass ($XCoM$) and the Base of Support (BoS) edges. First, the soundness of this metric in monitoring gait stability is proven. Experiments on 25 healthy individuals show that the median value of Pearson's correlation coefficient (p-value < 0.05) remained high during the forward walk for all subjects. Next, a correlation-based variable admittance (CVA) controller is implemented, whose parameters are tuned to physically support users when a gait perturbation is detected (i.e. low values of Pearson's correlation coefficient). To validate this approach, 13 healthy subjects were asked to compare our controller with a force threshold-based (FVA) one. The CVA controller's performance in discriminating stable and perturbed gait conditions showed a high sensitivity value, comparable to FVA, and improved performance in terms of specificity. The number of false and missed detections of gait perturbation was considerably reduced, independently of walking speed, exhibiting a higher level of safety and smoothness compared to the FVA controller. Overall, the outcome of this study gives promising evidence of the proposed metric capability in identifying user stability and triggering WANDER's assistance.**

Received 23 August 2024; accepted 6 December 2024. Date of publication 6 January 2025; date of current version 20 January 2025. This letter was recommended for publication by Associate Editor Tom Verstraten and Editor Jee-Hwan Ryu upon evaluation of the reviewers' comments. This work was supported by INAIL, BRiC LABORIUS Project ID 57. *(Corresponding author: Andrea Fortuna.)*

This work involved human subjects or animals in its research. Approval of all ethical and experimental procedures and protocols was granted by Azienda Sanitaria Locale (ASL) Genovese N.3 under Application No. IIT_HRII_SOPHIA 554/2020.

Andrea Fortuna is with the Human-Robot Interfaces and Interaction Laboratory, Istituto Italiano di Tecnologia, 16163 Genoa, Italy, and also with the Department of Electronics, Information and Bioengineering, Politecnico di Milano, 20133 Milan, Italy (e-mail: andrea.fortuna@iit.it).

Marta Lorenzini, Younggeol Cho, Robin Arbaud, and Arash Ajoudani are with the Human-Robot Interfaces and Interaction Laboratory, Istituto Italiano di Tecnologia, 16163 Genoa, Italy.

Stefano Filippo Castiglia is with the Department of Medical and Surgical Sciences and Biotechnologies, Sapienza University of Rome, 00185 Latina, Italy.

Mariano Serrao is with the Department of Medical and Surgical Sciences and Biotechnologies, Sapienza University of Rome, 00185 Latina, Italy, and also with the Movement Analysis Laboratory, Policlinico Italia, 00162 Rome, Italy.

Alberto Ranavalo is with the Department of Occupational and Environmental Medicine, Epidemiology and Hygiene, INAIL, 00040 Rome, Italy.

Elena De Momi is with the Department of Electronics, Information and Bioengineering, Politecnico di Milano, 20133 Milan, Italy.

Digital Object Identifier 10.1109/LRA.2025.3526444

***Index Terms*—Physically assistive devices, human and humanoid motion analysis and synthesis, sensor-based control.**

I. Introduction

FALLS are the leading cause of injuries and deaths among senior adults (i.e., people over 65 years of age) resulting in over 36,000 deaths, more than 1.8 million treat and release emergency department visits, and almost 1 million hospitalizations per year in the United States. The direct consequence is considerable costs for the National Health System that amount to $50 billion per year spent on the care and assistance of people following accidental falls [1]. To reduce the incidence of falls, it is crucial to preserve and encourage mobility in the elderly and adults with chronic conditions. Indeed, physical inactivity leads to muscle weakening, which perilously increases the risk of falls and fosters the onset of various diseases and health issues. These aspects highlight the need to provide fragile individuals with an agile and adaptable assistive device to ensure physical and psychological safety while promoting motor activity.

For this purpose, many mechanical structures for gait assistance have been proposed (e.g., walkers and canes). Nevertheless, the traditional tools suffer from several drawbacks, such as requiring sufficient force to move and handle the device, lack of adaptability with human motion and not providing robust support for user stability. Hence, more advanced robotic-assisted devices have recently attracted attention as an alternative. They mainly consist of two categories: robotic cane or smart walkers [2], [3] and Overground Walking Platforms (OWPs) [4], [5]. The first category features convenient reduced dimensions but requires the user to steer the device and cannot provide robust support in case of falls. On the other hand, OWPs provide partial body weight support (BWS) by securing the users to their structure and do not require the use of arms. However, they are bulky and have limited maneuverability, which binds their usage in healthcare settings.

To promote the usability of robotic-assisted walking aids in both clinical and domestic environments, emphasis should be placed on developing agile, practical, and reduced-dimension devices. A growing research effort is arising [6], [7], [8]. In this direction, a novel Walking Assistive omNi-Directional Exo-Robot (WANDER) was introduced in our previous work [9], where we maximized users' comfort while minimizing energy consumption thanks to the system's personalization. However, these features are not enough to ensure the users' safety and stability. Such requirements involve the early detection of potentially dangerous events (e.g., falls, loss of senses/balance, gait perturbation, etc.) and the implementation of control strategies

that allow users' support. To fulfill this demand, we present a novel metric for online quantifying the dynamic stability of human gait, and, based on this metric, provide the user with assist-as-needed support while using WANDER.

II. Related Works

The basic challenge in designing a control approach for fall-preventive assistive devices is to select a proper metric for the early detection of falls. Despite extensive research efforts, there is no standardized and quantitative method for assessing or scoring the dynamic stability of human locomotion [10], [11]. The loss of human balance from a standing position in static conditions has been extensively studied, but this model does not apply to walking due to its dynamic nature. Some techniques that offer similar extensions for evaluating dynamic gait stability can be found in the literature. In this section, we provide an overview of the state of the art, considering both the walking cases without and with gait-assistive devices.

A. Gait Stability Metrics Without Assistive Devices

The eXtrapolated Center of Mass ($XCoM$) is defined as [12]

$$XCoM = CoM + \frac{CoM'}{\sqrt{g/l}} \tag{1}$$

where l is the leg length [m], g is the gravity acceleration and CoM' is the derivative in time of Center of Mass (CoM). The $XCoM$ extends the classical condition for static equilibrium of an inverted pendulum and poses the CoM over the Base of Support (BoS) by adding a linear function of the velocity of the CoM to the CoM position. In [12], the *margin of stability* is defined by the relative position between the $XCoM$ and the anterior limit of BoS. However, according to this formulation, normal walking would be identified as a loss of balance since the $XCoM$ violates the stability margin criteria for most of the gait cycle [13]. This model could be successfully used to simulate walking, turning, and stopping [12] and can provide a quantitative comparison between pathological and healthy subjects [14], but this differs from predicting the probability of falls, and such studies have yet to be conducted.

In [15], the authors quantify the forces needed to stop the Center of Pressure (CoP) motion in the direction of the BoS edges (stabilizing force), and the force needed to bring the CoP outside the BoS (destabilizing force). An index of stability is then calculated by dividing the two forces. However, when computing the destabilizing force, movement speeds and accelerations are not considered. Thus, this metric can be applied only in static conditions and results too simplistic for dynamic walking [11]. The Foot Placement Estimator (FPE) [16], [17] estimates where the foot should be placed to guarantee a stable gait after the transition from one leg to the other. However, the findings of [16] demonstrate that metric accuracy systematically varies with different walking speeds, whereas [17] assesses the method through experiments involving a single subject. To the best of our knowledge, no observational studies have been conducted to date that predict the probability of falling in humans using the FPE method. Lastly, metrics from dynamical systems theory, such as the Maximum Lyapunov Exponent (MLE) and Maximum Floquet Multiplier (MFM) assess gait stability using metrics based on the time series data of kinematics and/or gait parameters. These methods, however, require expensive, cumbersome sensors and involve computationally demanding processes, which are typically conducted offline on pre-recorded data [18], [19] and are not suitable for real-time users' stability assessments.

B. Gait Stability Metrics Using Assistive Devices

Different studies can be found in the literature to assess user stability while walking with gait assistive devices.

For example, in [6], [13], and [20] methods based on a threshold on trunk velocity, acceleration, and applied forces are proposed. If the selected threshold is overcome, an unbalanced gait is detected. However, finding a suitable threshold for all the subjects is not trivial. Indeed, it was found people may apply high pushing forces even when their walk is stable, thus reducing the method's effectiveness. In [13], they attempt to address this issue by proposing a method based on a continuous version of the margin of stability. However, this approach relies on the strong assumption that stride length and duration remain constant over time. Furthermore, the latter study and the device in [8] do not present a control mechanism to assist the user in regaining stability, whereas in studies [6] and [20], the device immediately stops if the defined thresholds are exceeded, even if a modular intervention from the robot to correct the instability is more appropriate than a complete stop [6].

This letter aims to address current state-of-the-art limitations by proposing a novel metric that quantitatively online monitors the user's stability while walking with WANDER, enabling the delivery of suitable assistive support adaptively. Combining information from the insole sensors worn by the users and a 2D LiDAR, the person BoS and $XCoM$ are reconstructed. Then, the correlation between the variations of BoS and $XCoM$ in the Antero-Posterior (AP) plane is studied to assess the stability during walking. Finally, a variable controller that adapts based on user stability, providing assist-as-needed support, is tested on WANDER and compared to a state-of-the-art approach.

III. Hardware Overview

A. WANDER

The assistive device considered in this study is shown in the green block of Fig. 1. Its base consists of a velocity-controlled Robotnik SUMMIT-XL STEEL mobile platform with three degrees of freedom (DoFs), i.e., able to move in longitudinal and lateral directions and rotate in place. A structure of aluminum profiles is mounted on top of the mobile base and a LaxOne 6-axis force/torque (FT) sensor (Bota Systems, Zürich, Switzerland) is assembled in the middle of the horizontal profile. The FT sensor is placed between the structure and the user, who is coupled to the latter through a lumbar support at the pelvis level. Its vertical location on the structure can be adjusted to fit the height of each individual. By using this pelvic interface (sensor plus lumbar support), the forces and torques exerted by the user on the device can be detected. The overall dimensions of WANDER are $97.8 \times 77.6 \times 51$ [cm] and the weight is 150 [kg]. WANDER is also equipped with a reliable wireless emergency button.

B. LiDAR System

To estimate the CoM position and evaluate its relationship with BoS according to the proposed method, the detection of

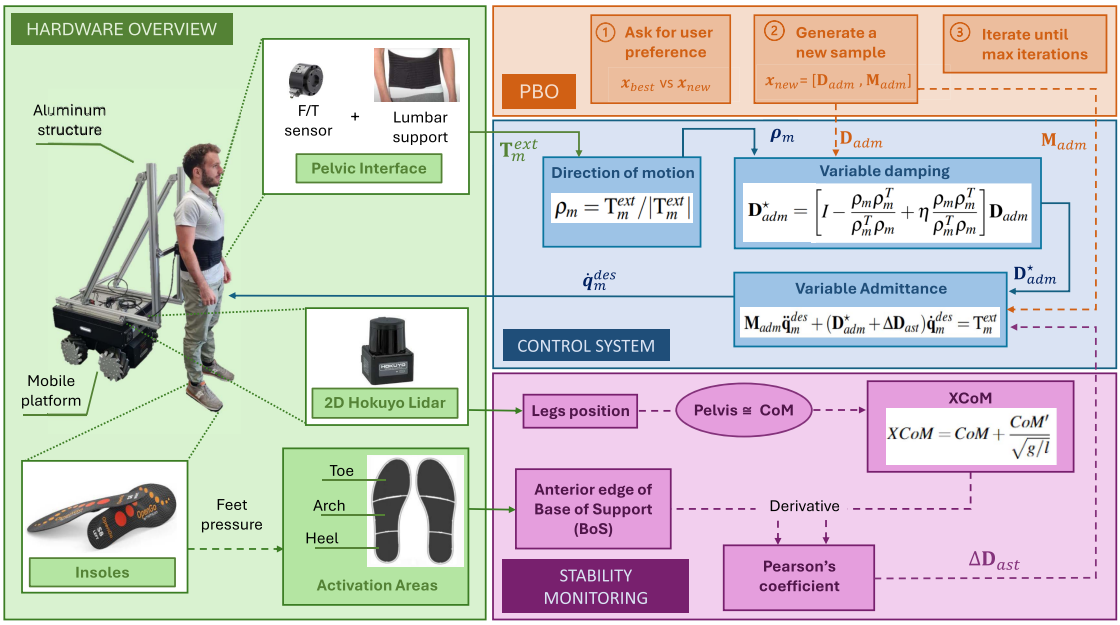

Fig. 1. Overview of WANDER and the underlying framework including hardware components (green block), Preference Based Optimization (PBO) procedure (orange block), control system (light blue block), and user stability assessment method (purple block).

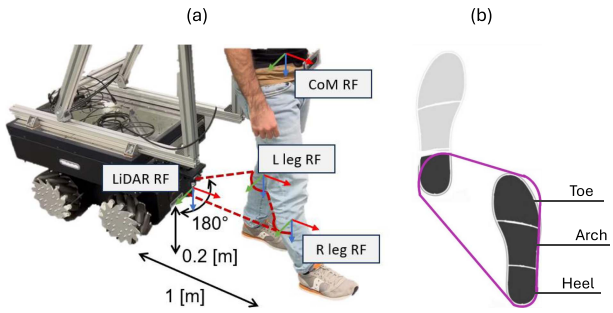

Fig. 2. (a) Details of the used Reference Frames (RFs): i) the LiDAR sets the global RF; ii) legs RFs are placed in the center of points cloud's circumferences; iii) CoM RF is in the middle point of the legs. (b) Example of BoS construction The subdivision of foot areas is also illustrated.

users' legs is required (details in Section IV). A 2D Hokuyo laser sensor mounted on the front side of WANDER at a height of 20 [cm] from the ground is used to detect the point clouds of the objects within the laser field of view. Then, the tracking technique presented in [21] allows us to estimate and track the legs' movement. The max detection distance for the laser is set to 1 [m], while the detection angle ranges from $-90°$ to $+90°$ at 40 [Hz]. The reference system of LiDAR is adopted, in this letter, as the global reference system (see Fig. 2).

C. Insoles System

For the computation of BoS, the Moticon OpenGo insoles were used. The system has 16 sensors per insole providing pressure for each sensor [N/cm^2], acceleration along x,y,z axes [g], angular rate $\omega_x, \omega_y, \omega_z$ [dps], CoP position and total vertical force [N]. These data were recorded with a frequency of 50 [Hz] and down-sampled in the controller loop to be synchronized with LiDAR's data. Insoles from 42 to 45 EU were used to cover multiple users' shoe sizes. Similar to [22], a pressure cell is considered active when the measured pressure is greater than 2.0 [N/cm^2], excluding low-intensity pressure peaks corresponding to the pressure measurement noise.

IV. Stable Walking Monitoring

In this section, the method to monitor user stability, represented in the purple block of Fig. 1, is explained. Experimental data on human gait suggest some proportionality of the center of mass and its speed (i.e., $XCoM$) and the movement of the feet in the next step [23]. At each gait step, people move into a phase of unbalance that is subsequently recovered by taking the next step. We therefore expect, during a steady walk, the fluctuations of the BoS edges to be connected to the $XCoM$. Based on that, we hypothesized that the correlation between the $XCoM$ and the BoS front edge could provide a potential criterion for discriminating between stable and unstable conditions during human gait. The methods for computing the two signals are first introduced, followed by an explanation of the approach proposed to relate them.

A. XCoM and BoS Computation

1) XCoM: In this letter, we assumed that CoM movement can be approximated by the movement of the pelvis [13], [24]. This assumption is reasonable in the proposed application since relative movements between body links are minimal due to the coupling between the user and WANDER. The movement of the pelvis is then reconstructed as the motion of the midpoint between the legs [3], detected at each instant by the LiDAR. Once the CoM is obtained, the $XCoM$ can be computed according to (1).

2) BoS: The sensors of each OpenGo insole were divided into heel, arch, and toe subgroups based on their location (Fig. 2(b)). Each area is considered active in the BoS construction if at least one of its pressure cells is active for more than one second. After identifying the active areas of each foot

individually, the latter were connected geometrically to obtain the total BoS (Fig. 2(b)).

B. XCoM - BoS Relationship

In this work, the Pearson coefficient between $XCoM$ and the anterior edge of BoS is used as the metric for assessing the correlation between them. This parameter quantifies the linear association between two data series, ranging from $+1$ (i.e., direct relationship) to -1 (i.e., inverse relationship). In sum, the Pearson coefficient captures the similarity between the absolute values of two signals, giving an idea of their overall relationship. On the other hand, the correlation between the derivatives of two signals offers a more detailed perspective on their rate of change over time, focusing on their dynamic behavior. Since we are more interested in the latter, Pearson's coefficient was calculated between the $XCoM$ and BoS derivatives. At every iteration, the first step to obtain Pearson's coefficient is the computation of signals' derivatives, and then the resultant $XCoM'$ and BoS' are filtered to remove noise measurements. Details about filtering choices are provided in Section VI-A. Next, the cross-correlation of a moving time window (with a number of samples equal to K) is calculated as

$$(XCoM' \star BoS')[n] = \sum_{h=0}^{K-1} \overline{XCoM'[h]} \cdot BoS'[h+n], \quad (2)$$

where $\overline{XCoM'[h]}$ is the conjugate of derivative $XCoM'$ at time sample h and $BoS'[h+n]$ is the BoS derivative shifted of n samples wrt h. Given the cross-correlation, it is possible to obtain the delay $n^\star$ as the maximum value registered for the given time window. Finally, the Pearson coefficient is calculated between the two shifted signals as

$$r = \frac{\sum (XCoM' - m_X)(BoS'[n^\star] - m_B)}{\sqrt{\sum (XCoM' - m_X)^2 \sum (BoS'[n^\star] - m_B)^2}}, \quad (3)$$

where m_X and m_B are the mean of vectors $XCoM'$ and BoS', computed online in the considered time window.

V. Variable Admittance Controller

In this section, the control algorithm developed to ensure the system's transparency with human movements [9] in stable walk and to provide assistance in case of gait perturbation (blue block in Fig. 1) is briefly described.

The user's intention in terms of force/torques (detected by the FT sensor) can be translated into desired velocities through an admittance controller, making WANDER compliant with human motion. The underlying dynamic relationship can be described by the following admittance model

$$\mathbf{M}_{adm}\ddot{\mathbf{q}}_m^{des} + (\mathbf{D}_{adm}^\star + \Delta\mathbf{D}_{ast})\dot{\mathbf{q}}_m^{des} = \mathrm{T}_m^{\mathrm{ext}}, \quad (4)$$

where $m = 3$ is the number of DoFs, representing two translational and one rotational movement of the base. $\ddot{\mathbf{q}}_m^{des}$ and $\dot{\mathbf{q}}_m^{des}$ are the desired accelerations and velocities, respectively. $\mathrm{T}_m^{\mathrm{ext}} = [F_x, F_y, \tau_z]$ are the detected external forces and torques, which are extracted and mapped from the 6D FT sensor data. This information is used to compute the directional damping matrix $\mathbf{D}_{adm}^\star$, as reported in the blue block in Fig. 1, to decrease the resistance along the direction of motion facilitating the user's movements. $\mathbf{M}_{adm}$ and $\mathbf{D}_{adm}$ are the diagonal positive definite matrices of virtual mass and damping in Cartesian coordinates

$$\mathbf{M}_{adm} = \begin{bmatrix} M_x & 0 & 0 \\ 0 & M_y & 0 \\ 0 & 0 & J_z \end{bmatrix}, \quad \mathbf{D}_{adm} = \begin{bmatrix} D_x & 0 & 0 \\ 0 & D_y & 0 \\ 0 & 0 & D_z \end{bmatrix},$$

where $M_{x,y}$ and $D_{x,y}$ are optimal mass and damping in the horizontal axes, J_z is the moment of inertia and D_z is the rotational damping. $\mathbf{D}_{adm}$ is used in the computation of $\mathbf{D}_{adm}^\star$. WANDER is designed to be freely moved by the user and maintain its position if no forces are applied. This is why we omit the stiffness term in (4). The parameters' optimal values are obtained for each participant by using a user preference-based optimization (PBO) procedure (orange block in Fig. 1). Details can be found in [9].

A. Correlation-Based Variable Admittance Controller

Building on top of this controller, an assistive strategy is implemented to help the user regain stability. When the proposed metric detects a perturbed gait, the Correlation-based Variable Admittance (CVA) controller increases $\Delta\mathbf{D}_{ast}$, enhancing resistance in the direction of motion and enabling the user to restore stability. To provide assist-as-needed support, the robotic assistive device's intervention must be proportional to the level of instability. If the user is walking stably, maintaining the system's mechanical transparency is crucial, so the additional assistance level remains at zero. Conversely, if a minor disturbance occurs during gait, the assistance level should increase modestly without being overly intrusive. In the presence of a significant perturbation, a more robust intervention is required to re-stabilize the gait. Based on [25] the domain of Pearson's coefficient is divided into three ranges of correlation: *low* i.e., $r < 0.4$, *weak* i.e., $0.4 \leq r < 0.6$ and *high* i.e., $r \geq 0.6$. The three ranges represent the high, minor, and null levels of gait perturbation, respectively. The level of assistance provided to the user will be calculated accordingly. To obtain $\Delta\mathbf{D}_{ast}$, we implement the following function

$$\Delta\mathbf{D}_{ast}(t) = \begin{cases} e^{\alpha T_1} - 1 \in [0, \mathbf{D}_{\mathrm{maxL}}] & \text{if } r < 0.4, \\ m_1 \cdot d \cdot K_t \in [0, \mathbf{D}_{\mathrm{maxW}}] & \text{if } 0.4 \leq r < 0.6, \\ -m_2 \cdot T_2 \in [0, \mathbf{D}_{\mathrm{maxL}}] & \text{if } r \geq 0.6. \end{cases} \quad (5)$$

where T_1 is the interval between initial time of perturbation and current time, $d \in [0, 0.2]$ is the difference between $high$ correlation threshold and current Person's coefficient, $\mathbf{D}_{\mathrm{maxL}}$ and $\mathbf{D}_{\mathrm{maxW}}$ are the maximum damping values selected for the *low* and *weak* range, respectively. The third equation of the system, where T_2 is the interval between the end of perturbation and current time, smoothly brings back the value of $\Delta\mathbf{D}_{ast}$ to zero when no perturbation is detected. The parameters m_1, K_t and m_2 are computed as follows

$$\begin{cases} m_1 = \mathbf{D}_{\mathrm{maxW}}/max(d), \\ K_t = \beta t_1 \\ m_2 = (\mathbf{D}_{\mathrm{maxW}} - \mathbf{D}_{adm})/\gamma \end{cases} \in [0,\ 1]. \quad (6)$$

α, β and γ in (5) and (6) are chosen to reach the maximum and zero assistive $\Delta\mathbf{D}_{ast}$ value in the desired time amount during low, $weak$ and $high$ correlation, respectively.

TABLE I
PARAMETERS SELECTED FOR THE CONTROLLER AND $\Delta\mathbf{D}_{ast}$ FUNCTION

Parameter	Value	Rationale
J_z	$0.33M_{x,y}$	Empirical
D_z	$0.33D_{x,y}$	Empirical
η	0.7	Empirical
$M_{x,y}$	$\in [10, 100]$	9% of system mass [29], Empirical
$D_{x,y}$	$\in [40, 200]$	Empirical
$\mathbf{D}_{maxL}$	400	$2 \cdot max(D_{x,y})$
$\mathbf{D}_{maxW}$	200	$max(D_{x,y})$
$\mathbf{D}_{act}$	40	$0.1 \cdot \Delta\mathbf{D}_{maxW}$
α	64.0	Empirical
β	3.0	Empirical
γ	8.0	Empirical

B. Force-Based Variable Admittance Controller

The proposed method is compared with a variable admittance controller based on force threshold (FVA), similar to the approach described in [6] and [20]. If the measured force in the moving direction exceeds the threshold, an unbalanced condition is detected. The assistive damping is computed as

$$\Delta\mathbf{D}_{ast}(t) = \begin{cases} e^{\alpha t} - 1 \in [0, \mathbf{D}_{\text{maxL}}] & \text{if } f > f_{th}, \\ -m_2 \cdot t \in [0, \mathbf{D}_{\text{maxL}}] & \text{if } f \leq f_{th}. \end{cases} \quad (7)$$

The parameters' values are reported in Table I while the force threshold is different for each user and its computation is described in Section VI-C.

VI. EXPERIMENTAL CAMPAIGN

Two experimental sessions were conducted. In the first phase, the proposed metric's capability to assess user stability while walking with WANDER was evaluated. In the second phase, subjects were asked to self-perturbate their gait (details will follow), and the performance of the proposed CVA controller was validated and compared with the FVA controller. The protocol was approved by the ethics committee Azienda Sanitaria Locale (ASL) Genovese N.3 (Protocol IIT_HRII_SOPHIA 554/2020). Written informed consent was obtained from the participants.

A. Parameters Settings

To compute Pearson's coefficient, we defined a moving time window with K = 80 samples and a significance level equal to 0.05. Regarding signal filtering, a second-order Butterworth filter was applied to $XCoM'$ and BoS' separately. This filter is commonly used, with cut-off frequencies between 3 and 10 Hz, for filtering biomechanical signals [26], [27] and has been proven robust with derivatives of signals. In our framework, a cut-off frequency of 4 Hz was selected to achieve a good balance between minimizing signal distortion and effectively removing noise. It should be noted that, in addition, we low-pass filtered the correlation signal to eliminate peaks with a duration of less than 0.3 seconds. This means that the controller is activated when the instability exceeds the threshold duration. The selection of the latter was dictated by the physiological time response to gait perturbation reported to be > 0.3 [s] [28].

The values of all the controller's parameters are reported in Table I. The values of α, β used in (6) were chosen to reach the maximum damping value in approximately 0.1 sec and 0.3 sec during low and $weak$ correlation, respectively. γ instead was empirically chosen to gradually bring back $\Delta\mathbf{D}_{ast}$ to zero during

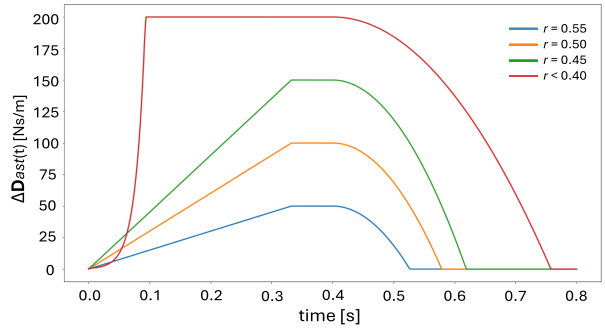

Fig. 3. Example of $\Delta\mathbf{D}_{ast}$ curves for a given $\Delta\mathbf{D}^{\star}_{adm}$ and fixed Pearson coefficients are reported as a function of time. The rising part of the curves corresponds to an increase in damping based on the current Pearson's coefficient, until the saturation value (constant segment of the curve). The descending part smoothly brings back $\Delta\mathbf{D}_{ast}$ to zero, when the perturbation is ended. The values of the curve $r < 0.4$ are scaled by 1:2 for better visualization.

high correlation. This choice can be attributed to the previously described assist-as-needed principle. If the perturbation was high, we required an intervention that was as reactive as possible, whereas if the perturbation was less significant, we preferred an intervention that increased over time. Based on the selected parameters, examples of increase and decrease of $\Delta\mathbf{D}_{ast}$ over time for a given initial $\mathbf{D}^{\star}_{adm}$ and fixed values of Pearson's coefficient are reported in Fig. 3.

B. Stability Metric Evaluation

1) Protocol: 25 healthy subjects (age: 28.08 $\pm$ 2.31 years; mass 77 $\pm$ 6.14 [kg] and height 181 $\pm$ 7.17 [cm]) were recruited. The pelvic interface was adjusted according to each participant's height and then, the subjects were connected to WANDER to obtain a tight coupling without affecting the users' comfort. First, the subject's custom parameters were determined using the PBO procedure [9]. Next, each subject was asked to walk straight in a normal fashion for 7 [m] for 12 trials.

2) Analysis: Pearson's correlation coefficient was computed between $XCoM'$ and BoS' during each trial. To test the normality of its distribution, the Shapiro-Wilk test was performed since the restricted dataset dimension (i.e., num sample < 5000), with a p-value equal to 0.05. Then, the trend of its value across subjects was analyzed.

C. Assistive Controller Evaluation

1) Protocol: In this second phase, we recruited only subjects who could guarantee high correlation values while walking straight with WANDER, i.e., who satisfied, in the first phase, the following condition on Pearson's coefficient:

$$r \geq 0.4 \ \ \forall \ \ t \in [0, t_{\text{end}}] \quad (8)$$

where t_{end} is the final instant of the trial. This choice was made to comply with the controller activation requirements described in (5). Further discussion will follow in Section VIII. Hence, 13 healthy subjects (age: 29.75 $\pm$ 2.68 years; mass 75.67 $\pm$ 6.14 [kg] and height 180 $\pm$ 7.17 [cm]) were selected. As a first step, a calibration trial was performed to determine the subject-specific threshold f_{th}. Subjects were asked to walk in a normal fashion without any perturbation, the forces detected by the FT sensor were recorded, and the maximum value was selected. After the calibration, 12 trials per subject were conducted in which the participants were asked to walk straight for 7 [m]. In

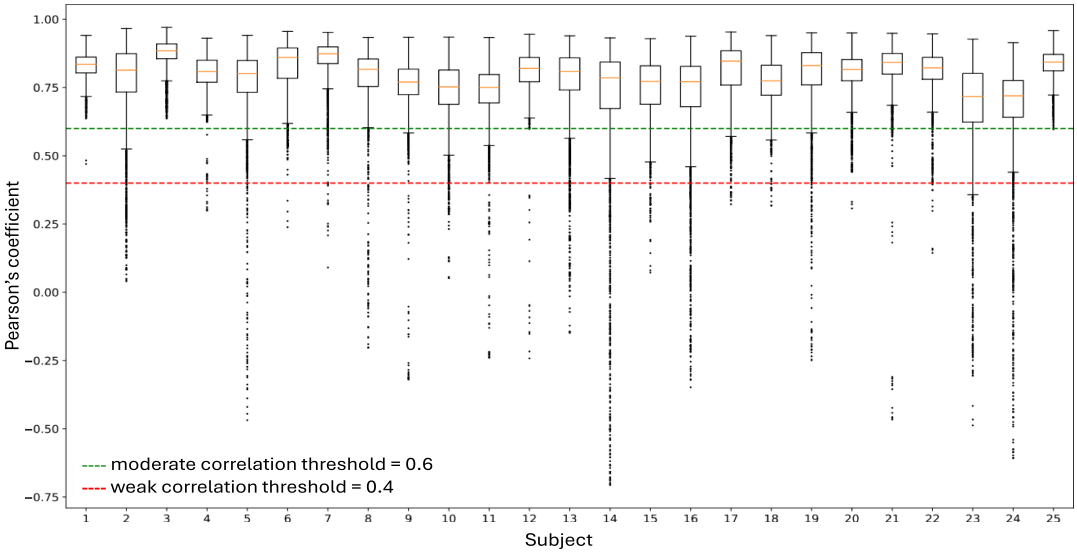

Fig. 4. Results of stability metric evaluation: the data for each subject include the correlation values measured across all 12 trials conducted by that subject. The figure shows a median Pearson's correlation coefficient greater than the moderate threshold ($r = 0.6$) and a first quartile greater than the low correlation for all the subjects.

9 of them, the *self-perturbation* trials (SPT), they were asked to self-perturb the gait following an acoustic signal, randomly generated along the path. The other 3, the *increasing speed* trials (IST), were performed by asking the subjects to adopt an increasing walking speed from the first (*v1*) to the latter trial (*v3*). The execution of all these trials was randomized and the described protocol was repeated with both controllers.

To standardize the gait stability evaluation, subjects were instructed to self-induce perturbations during walking, according to the protocol described in [30]. In particular, they were asked to freeze their gait during the swing phase, after the acoustic signal, and 'try to step as fast as possible' in subsequent steps.

2) Analysis: The controllers' performance in discriminating and managing stable and perturbed gait conditions was evaluated using quantitative and qualitative metrics. As quantitative metrics the activation time after the acoustic signal Δt_{act}, Sensitivity (Se), Specificity (Sp), and their geometric mean (G_mean) [6] were computed. The first can be measured as

$$\Delta t_{\text{act}} = t(\Delta \mathbf{D}_{ast} = \mathbf{D}_{\text{act}}) - t_{sig}, \tag{9}$$

where t_{sig} is the time of the acoustic signal and $t(\Delta \mathbf{D}_{ast} = \mathbf{D}_{\text{act}})$ is the time instant when the assistive damping reaches the activation threshold. It is important to mention that this time includes both the user's reaction time to the acoustic signal, the freezing of the gait phase, and the activation time of the controller following the perturbation. If the assistive damping reaches the activation threshold, following a perturbation during *self-perturbation* trials, it is considered a correctly detected perturbation (true positive TP). On the other hand, if the damping does not reach $\mathbf{D}_{\text{act}}$ during *increasing speed* trials, this is a correctly non-detected perturbation (true negative TN). Based on that, Se, Sp, and G_mean were computed:

$$Se = \frac{TP}{tot\ SPT}; \quad Sp = \frac{TN}{tot\ IST}; \quad G\_mean = \sqrt{Se \cdot Sp}$$

In addition, to get a deeper insight into the detection capability of the two approaches, false (FD) and missed (MD) detections of the perturbation across all the trials were analyzed.

TABLE II
CVA AND FVA CONTROLLERS' QUANTITATIVE METRICS

Control	Se [%]	Sp [%]	G_mean	FD (*increas. speed*)	*v1* [%]	*v2* [%]	*v3* [%]	MD	Mean Δt_{act} [s]
FVA	94	36	0.58	115 (87)	5	31	64	4	1.90
CVA	91	46	0.65	78 (31)	29	26	45	1	2.54

A custom questionnaire was proposed to evaluate the performance qualitatively. Each question evaluates the two controllers with a score from 1 to 5. The overall questionnaire can be found at: https://shorturl.at/BR4cq.

VII. RESULTS

A. Stability Metric Evaluation

The statistical test performed returns a non-gaussian distribution of the Pearson's coefficient for most of the subjects. Hence, the coefficient's median, first, and third quartile over 12 trials, which are shown through box plots for each subject in Fig. 4, were analyzed. It can be noted that the median value and the first quartile are greater than the $high$ correlation threshold $r = 0.6$ for all the subjects.

B. Assistive Controller Evaluation

In Table II the quantitative results are reported. The CVA controller exhibits better performance in terms of perturbation detection. Specifically, while the Se of the two methods is comparable, with the CVA, the Sp and G_mean are increased by 10% and 7% respectively and the number of FD is reduced by 32%, compared to the FVA. It can be noted that 76% and 40% of FD, for the FVA and CVA controllers, respectively, were recorded during the *increasing speed* trials. Moreover, the FVA exhibits an increasing trend from *v1* to *v3*, whereas no specific trend is observed for the CVA, which shows a decrease from

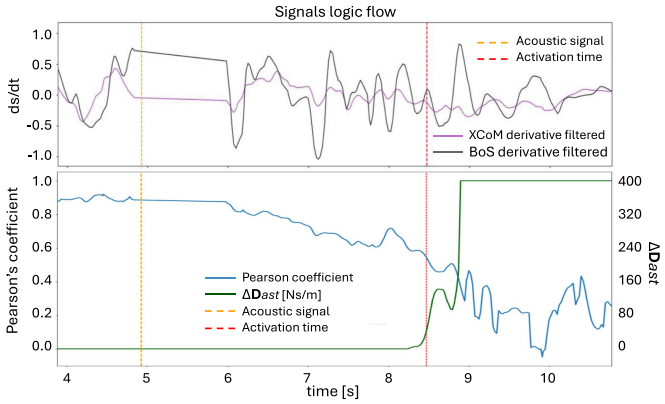

Fig. 5. The complete signals' logic flow is reported: in the image above the filtered derivatives are represented; in the image below, the drop in Pearson's coefficient and the consequent $\Delta\mathbf{D}_{ast}$ can be observed. The time between the acoustic signal (yellow line) and activation time (red line) comprises the user reaction time to start the gait's self-perturbation.

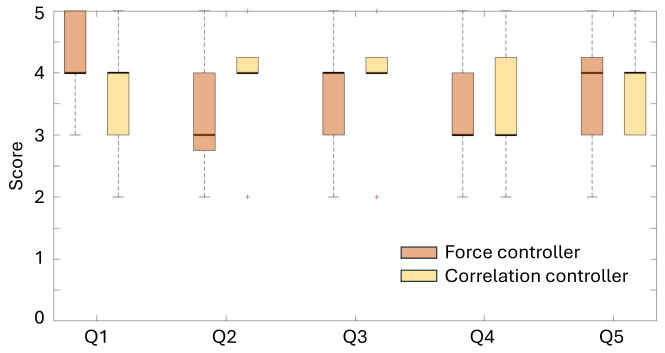

Fig. 6. Results of the custom questionnaire for all the subjects in the two experimental conditions (Force and Correlation control). The boxplots from question one (Q1) to five (Q5) are presented.

v1 to *v2* and an increase from the latter to *v3*. The number of MD is also decreased using CVA. Finally, the proposed CVA controller has a longer reaction time to perturbation events, that is, 0.64 seconds on average slower than the FVA controller. In Fig. 5 an example of *self-perturbation* trial is represented for one subject. In Fig. 6, the results of the custom questionnaire for all the subjects are reported through box plots for FVA and CVA controllers. The scores are reported so that high scores correspond to a positive outcome for each question. The mean score of the CVA controller is slightly higher than that of the FVA controller in Q2, Q3, and Q4, whereas the opposite is observed in Q1 and Q5. However, no statistical relevance is measured in any of the questions.

VIII. Discussion

The results presented in Section VII-A show that the value of the correlation between $XCoM'$ and Bos' is high for all subjects while walking straight, suggesting that the proposed metric can be successfully used to identify a stable gait condition. On the other hand, some subjects occasionally reported values of Pearson's coefficient below the weak correlation threshold $r = 0.4$. This undesirable behavior may be caused in part by the level of confidence in walking with the assistive device.

Indeed, the first-time use of the system may influence the walking style differently from person to person. Participants were also instructed to avoid crossing their legs while walking, as this could impede the LiDAR from tracking the legs, thereby compromising the computations. This requirement might be more or less easily achievable depending on an individual's usual walking style. Similar observations were discovered in [6] where subjects experienced a change in gait parameters when being connected to the assistive device. This is why subjects who did not fulfill the condition in (8) were not involved in the controller evaluation. Biomechanical studies will be held to investigate the proposed metric further, while walking both with and without WANDER, also considering the familiarization effect. As a result, the number of subjects in the correlation study will be increased, enabling the evaluation of the metric on a larger dataset.

Another limitation of the method is represented by the assumption that CoM is rigidly coupled to WANDER and located at the midpoint between the two legs. Indeed, in the case of oscillations at the user-device interface, the device movement no longer represents the pelvis movement, causing a negative peak in the correlation value. To address this issue, a new version of WANDER is being developed in our laboratory with an innovative design aimed at enhancing the coupling interface and optimizing patient ergonomics. Additionally, assuming that CoM movement can be approximated with pelvis movement is reasonable but not always valid. By including in the control system a camera to improve the estimation of CoM (e.g., by monitoring the torso movement), the fall detection accuracy and the overall efficacy of the method in identifying and restoring users' instability can be enhanced.

Despite this, quantitative results presented in Section VII-B demonstrate that the proposed CVA controller achieved high performance in detecting true gait perturbation (i.e., Se value), comparable to that of the FVA. Instead, the CVA controller capability in identifying normal gait (i.e. Sp value) was greatly improved to FVA. Finally, the G_mean and the reduction of both FD and MD show an overall better performance of CVA controller. This indicates not only that smoothness is increased during normal walking, but also that a higher level of safety is provided in case of instabilities. Additionally, the analysis of the distribution of FD reveals that those related to the FVA controller are more concentrated in *increasing speed* trials. This issue is probably inherent to the intrinsic functioning of the controller. Indeed, since the detected forces are related to the walking speed, if the user increases the latter, the first increases as well, potentially exceeding the selected threshold. Conversely, the failures of the proposed method are distributed across all the trials, indicating that the CVA controller performance is independent of walking speed. The findings on the FVA controller are partially supported by [6] where the algorithm was tested under two protocols, yielding significantly different outcomes. In one protocol, the G_mean was 0.973, with sensitivity (Se) and specificity (Sp) of 94.7% and 100%, respectively, while the second protocol resulted in a G_mean of 0.717, with Se of 67.5% and Sp of 76.3%. However, the controller was evaluated with users' velocities reduced by the device, and, when tested with a patient, false positives occurred in all trials. In addition, this method can only provide the function of a complete stop of the user, while the proposed controller can deliver a modular intervention that allows an appropriate assistive force to correct the instability. On the other hand, the FVA controller is more responsive to perturbation events, exhibiting a shorter activation time than the CVA controller. We attribute this delay primarily to the multiple

filtering stages of the correlation signal, which introduce latency into the system. Enhancing the CoM estimation may also allow for a reduction in the signal filtering layers, thereby increasing the controller's responsiveness.

On the other hand, the FVA controller exhibits a shorter activation time than the CVA controller. We attribute this delay primarily to the multiple filtering stages of the correlation signal, which introduce latency into the system. Enhancing the CoM estimation may also allow for a reduction in the signal filtering layers, thereby increasing the controller's responsiveness.

Finally, since pathological conditions affect dynamic balance during walking [31], patients with motor dysfunctions (e.g., Parkinson's disease, ataxia) will be included in the next studies, enhancing the demographic diversity and proving the robustness of the method with the actual future users of WANDER.

IX. Conclusion

In this work, we introduced a novel metric to evaluate human stability during normal and perturbed gait conditions. We then presented a control strategy for the walking assistive device WANDER to enhance transparency during stable walking while providing physical support in case of perturbation.

The experimental results showed the effectiveness of our strategy in monitoring user stability and providing physical assistance after a gait perturbation. The proposed method improved the capacity to distinguish between stable and perturbed gait conditions compared to a force threshold-based controller from the literature, thereby improving movement smoothness and the safety of the assistive device.

References

[1] C. for Disease Control and Prevention, "Older adult fall prevention," 2022. Accessed: Apr. 12, 2023. [Online]. Available: https://www.cdc.gov/falls/index.html

[2] L. Ding et al., "Intelligent assistance for older adults via an admittance-controlled wheeled mobile manipulator with task-dependent end-effectors," *Mechatronics*, vol. 85, 2022, Art. no. 102821.

[3] S. Itadera and G. Cheng, "Admittance model optimization for gait balance assistance of a robotic walker: Passive model-based mechanical assessment," in *Proc. 2022 Int. Conf. Robot. Automat.*, 2022, pp. 7014–7020.

[4] N. A. Alias, M. S. Huq, B. S. K. K. Ibrahim, and R. Omar, "The efficacy of state of the art overground gait rehabilitation robotics: A bird's eye view," *Procedia Comput. Sci.*, vol. 105, pp. 365–370, 2017.

[5] D. Marks et al., "The Andago for overground gait training in patients with gait disorders after stroke-results from a usability study," *Physiother Res Rep*, vol. 2, no. 2, pp. 1–8, 2019, doi: 10.15761/PRR.1000128.

[6] L. Li et al., "Mobile robotic balance assistant (MRBA): A gait assistive and fall intervention robot for daily living," *J. NeuroEngineering Rehabil.*, vol. 20, no. 1, 2023, Art. no. 29.

[7] K. -R. Mun, Z. Guo, and H. Yu, "Development and evaluation of a novel overground robotic walker for pelvic motion support," in *Proc. 2015 IEEE Int. Conf. Rehabil. Robot.*, 2015, pp. 95–100.

[8] G. Aguirre-Ollinger and H. Yu, "Omnidirectional platforms for gait training: Admittance-shaping control for enhanced mobility," *J. Intell. Robotic Syst.*, vol. 101, 2021, Art. no. 52.

[9] A. Fortuna et al., "A personalizable controller for the walking assistive omNi-directional exo-robot (WANDER)," in *Proc. IEEE Int. Conf. Robot. Automat.*, 2024, pp. 3212–3218, doi: 10.1109/ICRA57147.2024.10611368.

[10] D. Hamacher, N. Singh, J. Van Dieën, M. Heller, and W. Taylor, "Kinematic measures for assessing gait stability in elderly individuals: A systematic review," *J. Roy. Soc. Interface / Roy. Soc.*, vol. 8, no. 65, pp. 1682–1698, Dec. 2011, doi: 10.1098/rsif.2011.0416.

[11] S.M. Bruijn, O.G. Meijer, P.J. Beek, and J. H. van Dieen, "Assessing the stability of human locomotion: A review of current measures," *J. Roy. Soc. Interface / Roy. Soc.*, vol. 10, no. 83, Jun. 2013, Art. no. 20120999, doi: 10.1098/rsif.2012.0999.

[12] A. L. Hof, "The 'extrapolated center of mass' concept suggests a simple control of balance in walking," *Hum. Movement Sci.*, vol. 27, no. 1, pp. 112–25, Feb. 2008.

[13] S. Page, K. -R. Mun, Z. Guo, F. A. Reyes, H. Yu, and V. Pasqui, "Unbalance detection to avoid falls with the use of a smart walker," in *Proc. 6th IEEE Int. Conf. Biomed. Robot. Biomechatronics*, 2016, pp. 1000–1005.

[14] A. -L. Simon, V. Lugade, K. Bernhardt, A. N. Larson, and K. Kaufman, "Assessment of stability during gait in patients with spinal deformity—A preliminary analysis using the dynamic stability margin," *Gait Posture*, vol. 55, pp. 37–42, 2017. [Online]. Available: https://www.sciencedirect.com/science/article/pii/S0966636217301091

[15] C. Duclos et al., "Destabilizing and stabilizing forces to assess equilibrium during everyday activities," *J. Biomech.*, vol. 42, no. 3, pp. 379–382, Feb. 2009. [Online]. Available: https://www.sciencedirect.com/science/article/pii/S0021929008005824

[16] M. Millard, D. Wight, J. McPhee, E. Kubica, and D. Wang, "Human foot placement and balance in the sagittal plane," *J. Biomechanical Eng.*, vol. 131, no. 12, Dec. 2009, Art. no. 121001.

[17] M. Millard, J. McPhee, and E. Kubica, "Foot placement and balance in 3D," *J. Comput. Nonlinear Dyn.*, vol. 7, no. 2, Apr. 2012, Art. no. 021015.

[18] C. Park and K. Park, "Dynamic stability of human walking in response to sudden speed changes," *Symmetry*, vol. 16, no. 1, 2024, Art. no. 26, doi: 10.3390/sym16010026. [Online]. Available: https://www.mdpi.com/2073-8994/16/1/26

[19] P. T. Chinimilli, S. M. Rezayat Sorkhabadi, and W. Zhang, "Assessment of human dynamic gait stability with a lower extremity assistive device," *IEEE Trans. Neural Syst. Rehabil. Eng.*, vol. 28, no. 3, pp. 669–678, Mar. 2020.

[20] C. Bühler, "Evaluation of the mobil walking & lifting aid," 2001. [Online]. Available: https://api.semanticscholar.org/CorpusID:218064633

[21] P. Balatti et al., "Robot-assisted navigation for visually impaired through adaptive impedance and path planning," in *Proc. IEEE Int. Conf. Robot. Automat.*, 2024, pp. 2310–2316.

[22] P. Morin, A. Muller, C. Pontonnier, and G. Dumont, "Evaluation of the foot center of pressure estimation from pressure insoles during sidestep cuts, runs and walks," *Sensors*, vol. 22, no. 15, 2022, Art. no. 5628. [Online]. Available: https://www.mdpi.com/1424-8220/22/15/5628

[23] M. Vlutters, E. H. F. van Asseldonk, and H. van der Kooij, "Center of mass velocity-based predictions in balance recovery following pelvis perturbations during human walking," *J. Exp. Biol.*, vol. 219, no. 10, pp. 1514–1523, May 2016. [Online]. Available: https://doi.org/10.1242/jeb.129338

[24] M. Schepers, E. H. F. van Asseldonk, J. H. Buurke, and P. H. Veltink, "Ambulatory estimation of center of mass displacement during walking," *IEEE Trans. Biomed. Eng.*, vol. 56, no. 4, pp. 1189–1195, Apr. 2009.

[25] J. D. Evans, *Straightforward Statistics for the Behavioral Sciences*. Pacific Grove, CA, USA: Thomson Brooks/Cole, 1996. [Online]. Available: https://www.scirp.org/reference/referencespapers?referenceid=1360433

[26] W. A. David, "Biomechanics and motor control of human movement," in *Biomechanics and Motor Control of Human Movement*. Hoboken, NJ, USA: Wiley, 2009, doi: 10.1002/9780470549148.

[27] F. Crenna, G. B. Rossi, and M. Berardengo, "Filtering biomechanical signals in movement analysis," *Sensors*, vol. 21, no. 13, 2021, Art. no. 4580. [Online]. Available: https://www.mdpi.com/1424-8220/21/13/4580

[28] A. L. Hof, S. M. Vermerris, and W. A. Gjaltema, "Balance responses to lateral perturbations in human treadmill walking," *J. Exp. Biol.*, vol. 213, no. 15, pp. 2655–2664, Aug. 2010.

[29] A. Lecours, B. Mayer-St-Onge, and C. Gosselin, "Variable admittance control of a four-degree-of-freedom intelligent assist device," in *Proc. 2012 IEEE Int. Conf. Robot. Automat.*, 2012, pp. 3903–3908.

[30] B. E. Maki and W. E. McIlroy, "The role of limb movements in maintaining upright stance: The "change-in-support" strategy," *Phys. Ther.*, vol. 77, no. 5, pp. 488–507, May 1997.

[31] M. Serrao et al., "Use of dynamic movement orthoses to improve gait stability and trunk control in ataxic patients," *Eur J. Phys. Rehabil. Med.*, vol. 53, no. 5, pp. 735–743, 2017.